A Simple Time-Domain Algorithm for Synchrophasor, Frequency and ROCOF Estimation

David Macii, Dario Petri
Department of Industrial Engineering
University of Trento
Trento, Italy
david.macii@unitn.it

Abstract – **The proliferation of distributed energy resources and plug-in electric vehicles is expected to change present distribution systems, thus stressing the role of measurement instrumentation enabling safe and flexible smart grid operation. In this context, Phasor Measurement Units (PMUs) are required to measure amplitude, phase, frequency and rate of change of frequency (ROCOF) of AC waveforms not only in steady state, but also, and above all, under dynamic conditions, while still ensuring extremely low measurement uncertainty and high reporting rates. In this paper a lightweight signal processing algorithm based on the so-called Teager's energy operator is adopted to measure amplitude, phase, frequency and ROCOF of AC waveforms in some of the testing conditions prescribed by the IEEE Standard C37.118.1-2011 and the IEEE Amendment C37.118.1a-2014. The reported analysis shows that the Teager's algorithm can provide high-rate and reasonably accurate measurement results under dynamic conditions. However, due to its sensitivity to wideband and narrowband disturbances, a preliminary band-pass filter is needed. In addition, instantaneous frequency and, above all, ROCOF estimates should be averaged to remove the residual effect of disturbances and to meet the limits reported in the IEEE Standards.**

Keywords – **Phasor Measument Unit (PMU), power system monitoring, signal processing, estimation uncertainty.**

I. INTRODUCTION

A Phasor Measurement Unit (PMU) is an instrument able to measure amplitude, phase, frequency and rate of change of frequency (ROCOF) of AC voltage or current signals at times synchronized to the Coordinated Universal Time (UTC) and with reporting rates in the order of tens of Hz [1]. Till now, PMUs have been mainly used for transmission systems monitoring, e.g., to support power system state estimation over wide geographical areas and to detect possible anomalous conditions or faults, thus triggering timely protection actions [2]. However, with the evolution of the so-called active distribution grids, the use of PMUs has become more and more appealing also at the distribution level. In this context, PMUs can be used, for instance, to detect and to locate possible faults [3], to evaluate the trade-off between distribution grid reliability and regulation market efficiency [4], and to monitor possible state fluctuations due to increasing photovoltaic penetration [5]. The integration of PMUs and Intelligent Electronic Devices compliant with the IEC Standard 61850 can indeed greatly support substation automation [6].

It is known that the metrological requirements of PMUs for distribution systems have to be stricter than those for transmission systems, particularly as far as phase measurements are concerned [7]. Indeed, the magnitude and angle phasor differences across distribution systems in steady-state conditions are usually much smaller than at the transmission level. On the other hand, the need to track synchrophasors as well as frequency variations under dynamic operating conditions (e.g., when power demand and supply change quickly) require high accuracy even in the presence of time-varying quantities. To this end, several innovative measurement techniques for PMUs have been proposed over the last few years to estimate electrical AC waveform parameters in dynamic conditions. Most of them rely on the idea to model synchrophasor variations over time using its Taylor's series truncated to the second- or third-order terms. In this way, synchrophasor magnitude and phase as well as fundamental frequency and ROCOF can be derived from the series coefficients, whose values can be estimated either in the time domain (e.g., through least-squares or weighted least-squares fitting of a data record [8], [9], possibly enhanced through a preliminary fundamental frequency estimation [10]), or in the frequency domain (e.g., by solving a linear complex-valued system [11]). The use of Taylor's series to model time varying phasors has been also extended to estimate harmonics parameters both in quasi steady-state conditions (e.g., through the so-called Taylor-Fourier Transform – TFT [12], [13]) and during fast transients [14]. Moreover, several researchers explored the possibility to further improve waveform parameters estimation in time-varying conditions through Kalman filters [15], [16], [17], or compressive sensing [18].

A well-known common issue to all estimators based on the Taylor's series synchrophasor model (particularly the TFT) is their considerable computational burden as the data record size grows. Even though this problem can be mitigated using real-valued equations and optimizing the number of harmonics included in the measurement model [19], alternative and simpler techniques would be definitely more suitable for low-cost embedded platforms (such as those adopted within the OpenPMU project [20]), which could promote the diffusion of PMUs over a large scale. In this respect, the Teager's algorithm (developed in the eighties to estimate the energy of

time-varying audio signals on-the-fly [21]) is able to estimate amplitude and frequency of dynamic signals with good accuracy, low computational burden, and sample-by-sample temporal resolution [22]. This is indeed the basic idea developed in this paper. In Section II the Teager's algorithm is briefly recalled along with the key expressions for fundamental frequency, amplitude, phase and ROCOF estimation. In Section III, the results of some preliminary simulations in the case of amplitude and phase modulated signals are reported. In Section IV, after a short discussion about the algorithm sensitivity to disturbances, two digital filters suitably designed to mitigate the effect of noise, harmonics and inter-harmonics in the *Class P* and *Class M* testing conditions specified in the IEEE Standard C37.118.1-2011 and in the Amendment IEEE C37.118.1a-2014 are described [23], [24]. In Section V, the results of exhaustive Monte Carlo simulations with and without averaging the estimated values of amplitude, phase, frequency and ROCOF are summarized and commented. Finally, Section VI concludes the paper.

II. Estimation Algorithm Description

A generic AC waveform acquired by a PMU at a sampling rate f_s can be modeled as

$$x(n) = X(n)\cos[\theta(n)] + \varepsilon_n(n) + \varepsilon_w(n) \qquad (1)$$

where:

- $X(n) = X\cdot[1+x_a(n)]$ is the time-varying amplitude of the AC waveform given by the superimposition of a constant value X and a modulating signal $x_a(n)$;
- $\theta(n) = 2\pi\frac{f}{f_s}n + x_p(n) + \theta_0$ is the instantaneous phase of the AC waveform at time n/f_s. This is given by the sum of the initial phase θ_0, a possible phase modulating signal $x_p(n)$, and the physiological angle increment due to the phasor rotation at frequency $f = f_0\cdot(1 + \delta)$, where f_0 is the nominal frequency (i.e., 50 Hz or 60 Hz) and δ represents a fractional off-nominal frequency deviations depending on the load conditions of the grid;
- function $\varepsilon_n(\cdot)$ represents the steady-state harmonics and/or inter-harmonics affecting the collected AC waveform;
- finally, $\varepsilon_w(\cdot)$ is a wideband noise modeling the disturbance contributions due to transducers, acquisition circuitry, and synchronization jitter [25].

Let us apply the discrete-time Teager's *energy operator* $\Psi[\cdot]$ defined in [22] to signal $x(n)$, i.e.

$$\Psi[x(n)] = x^2(n) - x(n-1)x(n+1). \qquad (2)$$

Assume that:

i. the bandwidth BW of $x_a(\cdot)$ and $x_p(\cdot)$ is much smaller than the fundamental frequency f;
ii. the modulation indexes associated with $x_a(\cdot)$ and/or $x_p(\cdot)$ are much smaller than 1;
iii. both narrowband and wideband disturbances are negligible (i.e. $\varepsilon_n(\cdot) \approx 0$ and $\varepsilon_w(\cdot) \approx 0$).

By replacing (1) into (2), the following approximate expression results, i.e. [22],

$$\Psi[x(n)] \approx X^2(n)\sin^2\left[2\pi\frac{f_i(n)}{f_s}\right] \quad \text{for} \quad |f_i(n) - f| \le BW. \quad (3)$$

Consider that, in power systems, assumptions i) and ii) above are generally met, unless some fault occurs. In fact, the values of amplitude modulation (AM) and phase modulation (PM) parameters are typically quite small [23], [24] a. Observe also that if amplitude and phase fluctuations are negligible [i.e. $x_a(\cdot) = x_p(\cdot) = 0$], expression (3) holds exactly and it is independent of time index n, even if f is affected by a nonzero static fractional off-nominal deviation δ.

By applying the Teager's energy operator $\Psi[\cdot]$ to the first-order time derivative of (1) estimated through the backward Euler method (i.e., $y(n) = x(n) - x(n\text{-}1)$), after a few algebraic steps and under the same assumptions i)-iii) listed above, it results that [22]

$$\Psi[y(n)] \approx 4X^2(n)\sin^2\left[\pi\frac{(f_i(n-\frac{1}{2}))}{f_s}\right]\sin^2\left[2\pi\frac{(f_i(n-\frac{1}{2}))}{f_s}\right]. \quad (4)$$

Again, (4) holds for $|f_i(n) - f| \le BW$ and turns into an exact expression (i.e., independent of n) for $x_a(\cdot) = x_p(\cdot) = 0$. Note that the backward difference introduces a ½ sample delay, whose effect on estimation results should be properly compensated. In this respect, by applying the Teager's energy operator $\Psi[\cdot]$ to the derivative of (1) computed using the forward Euler method, i.e. $z(n) = x(n+1) - x(n)$, the following dual expression results:

$$\Psi[z(n)] \approx 4X^2(n)\sin^2\left[\pi\frac{(f_i(n+\frac{1}{2}))}{f_s}\right]\sin^2\left[2\pi\frac{(f_i(n+\frac{1}{2}))}{f_s}\right]. \quad (5)$$

Therefore, by averaging (4) and (5), the respective systematic contributions due to the ±½ sampling period offsets are approximately cancelled out, i.e. [22]

$$\frac{\Psi[y(n)] + \Psi[z(n)]}{2} \approx 4X^2(n)\sin^2\left[\pi\frac{f_i(n)}{f_s}\right]\sin^2\left[2\pi\frac{f_i(n)}{f_s}\right]. \quad (6)$$

Ultimately, by computing the ratio between (6) and $2\Psi[x(n)]$, where $\Psi[x(n)]$ is given by (3), and using basic trigonometric properties, the fundamental frequency of the AC waveform is given by

$$f_i(n) \approx \frac{f_s}{2\pi}\arccos\left[1 - \frac{\Psi[y(n)] + \Psi[z(n)]}{4\Psi[x(n)]}\right]. \qquad (7)$$

Moreover, by replacing (7) into (3), the time-varying phasor amplitude is given by

$$X(n) \approx \sqrt{\frac{\Psi[x(n)]}{1 - \left[1 - \frac{\Psi[y(n)] + \Psi[z(n)]}{4\Psi[x(n)]}\right]^2}}. \qquad (8)$$

Finally, once $f_i(n)$ and $X(n)$ are known, still assuming that narrowband and wideband disturbances are negligible, the phasor instantaneous angle can be obtained from (1), i.e.

$$\theta(n) \approx \operatorname{acos}\left[\frac{x(n)}{X(n)}\right], \tag{9}$$

while the ROCOF can be estimated from the average of the backward and forward Euler differences of (7), which leads to

$$ROCOF(n) \approx \frac{f_s^2}{4\pi}\left\{\operatorname{acos}\left[1-\frac{\Psi[y(n+1)]+\Psi[z(n+1)]}{4\Psi[x(n+1)]}\right] - \operatorname{acos}\left[1-\frac{\Psi[y(n-1)]+\Psi[z(n-1)]}{4\Psi[x(n-1)]}\right]\right\}. \tag{10}$$

It is worth emphasizing that expressions (7)-(10) are very light from the computational point of view, since they require just 5 samples [i.e., $x(n\text{-}2)$, $x(n\text{-}1)$, $x(n)$, $x(n\text{+}1)$ and $x(n\text{+}2)$] and basic scalar algebraic and trigonometric functions to return sample-by-sample values of frequency, amplitude, phase and ROCOF, respectively. Therefore, the approach based on the Teager's energy operator in principle can provide high-rate results. However, in practice the computational burden is larger because a preliminary bandpass filter (which requires from tens to hundreds of Multiply-Accumulate operations) is needed to remove critical disturbances, a explained in Section IV. Observe that the forward Euler difference used to derive (7) and (10) makes the proposed approach formally noncausal. However, this problem can be easily addressed by introducing a 2-sample delay. Such a delay is definitely acceptable (i.e. much smaller than 1 power line cycle), since the sampling rate f_s is usually quite larger than f_0.

III. PROOF OF CONCEPT

The correct operation of the proposed approach under the assumptions reported in Section II (i.e. negligible disturbances and narrowband AM or PM signals) was proved through Monte Carlo simulations. The main simulation parameters are: f_s = 6.4 kHz, $X = \sqrt{2}$ p.u., f_0 = 50 Hz and $\delta = 0$. AM and PM were implemented using cosinusoidal signals, i.e. $x_a(n) = k_a\cos(2\pi f_a/f_s n + \varphi_a)$ or $x_p(n) = k_p\cos(2\pi f_p/f_s n + \varphi_p)$, included alternatively in (1). The modulating signal parameters (i.e., k_a = 0.1 and k_p = 0.1 rad with f_a and f_p ranging from 0 Hz to 5 Hz) were set in accordance with the maximum values reported in [24]. The initial phases of the fundamental and the modulating tones (i.e., θ_0, φ_a and φ_b) were generated randomly with a uniform probability within [0, 2π]. Globally, 50 waveforms of about 5 s each were used to evaluate estimation algorithm accuracy. Fig. 1 shows the maximum *Total Vector Error* (TVE), *Frequency Error* (FE) and *ROCOF Error* (RFE) computed over such repeated tests in the AM case (solid lines) and PM case (dotted lines), respectively, as a function of the modulating frequency. Observe that the TVE, FE and RFE values are negligible when the modulating frequency tends to zero. This is due to the fact that, as explained in Section II, expressions (3)-(5) hold exactly when

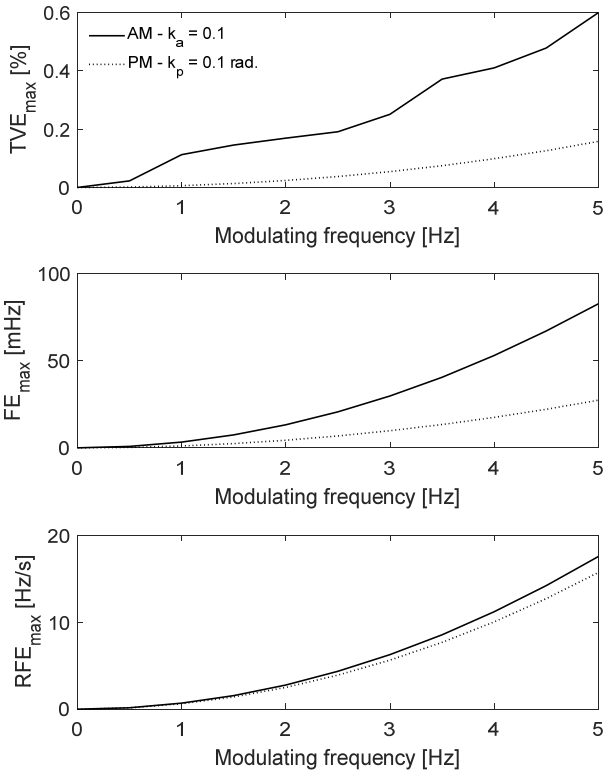

Fig. 1 – Maximum values of TVE, FE and RFE computed over 50 repeated trials under the effect of AM (solid lines) or PM (dotted lines) signals of given amplitude (i.e. k_a = 0.1 or k_p = 0.1 rad) and increasing frequency.

no AM or PM is present. On the contrary, when the modulating frequency increases, the approximation error affecting (3)-(5) grows as well. Consider that the frequency estimation based on (7) is more sensitive to AM than to PM. As a result, the estimation uncertainty in the AM case is worse and the gap between the TVE, FE and RFE curves tends to increase as the modulating frequency grows. However, while the TVE and FE values remain within reasonable limits, the RFE tends to grow much more quickly. This is due to the inherent higher sensitivity of ROCOF estimation based on (10) to noise and disturbances.

IV. SENSITIVITY TO DISTURBANCES AND SOLUTIONS

The preliminary results presented in Section III (particularly those related to ROCOF estimation) suggest that the algorithm based on the Teager's operator, although computationally simple and potentially very effective, could lead to poor results when the features of the input signal deviate significantly from assumptions i)-iii). The sensitivity of this algorithm to noise is indeed a known issue [22], and it is confirmed by further simulations (not reported here for the sake of brevity) performed in the same conditions described in Section III, but with noisy waveforms. In that case, assuming a Signal-to-Noise Ratio (SNR) of 60 dB (which is in line with the value determined experimentally in [25]), the TVE, FE and RFE values become huge (i.e., from 2 to 4 order of magnitude larger than those shown in Fig. 1), and, consequently, unacceptable for PMU applications. This problem can be

addressed by filtering the digitized sequence (1) prior to applying expressions (7)-(10). In particular, a zero-phase bandpass Finite Impulse Response (FIR) filter should be used to avoid that its phase response affect synchrophasor angle estimation. It is worth emphasizing that, unlike the model described in Annex C of the IEEE Standard C37.118.1-2011 [23], no low-pass filters after signal frequency down-conversion can be used in the case at hand. Indeed, the technique based on the Teager's energy operator can be successfully applied only to AC signals; otherwise accuracy of (7) drops. As a consequence, the filter must have a passband centered at f_0 and its bandwidth must be large enough not to affect the estimation of amplitude, phase, frequency and ROCOF when such quantities change over time. Moreover, the filter transition bandwidth has to be narrow enough to reduce second-order harmonics and out-of-band inter-harmonics to negligible levels. In addition, filter attenuation in the stopband has to be particularly large.

Based on the considerations above, two FIR filters were designed by adapting the general approach described in [26] to bandpass filters. The main features of both filters are summarized in Tab. I, while the magnitude of their frequency response is plotted in Fig. 2(a)-(b). The first filter is conceived for *Class P* (i.e., protection) applications and its impulse response is 3 power-line cycles long [23]. The second filter is instead intended for *Class M* (i.e., measurement) applications, which typically require higher accuracy [23]. This filter exhibits indeed a much longer impulse response (10 vs. 3 power line cycles), but it ensures a good rejection of possible out-of-band inter-harmonics. Two different optimization techniques were used to design either filter. The *Class M* filter results from a minimax optimization procedure based on the classic Parks-McClellan algorithm. In this way, the attenuation of both out-of-band inter-harmonics and harmonics is kept under tight control, at the expense of impulse response length. On the contrary, the *Class P* filter relies on least-squares error minimization.

This approach relaxes the ripple magnitude at the edges of the passband and the stopband (since out-of-band inter-harmonics are not considered in *Class P* PMU testing), but it ensures a narrower transition bandwidth and, consequently, a much shorter impulse response.

TABLE I – MAIN FEATURES OF TWO BANDPASS FILTER (FOR *CLASS P* AND *CLASS M* APPLICATIONS, RESPECTIVELY) DESIGNED PURPOSELY TO REMOVE POSSIBLE DISTURBANCES PRIOR TO APPLYING THE EXPRESSIONS (7)-(10).

Feature	*Class P*	*Class M*
Impulse response length [cycles]	3	10
Passband edge frequencies [Hz]	48.2 – 51.8	45.3 – 54.7
Stopband edge frequencies [Hz]	3 – 100	19.5 – 80.5
Max. passband ripple magnitude [dB]	0.015	0.0022
Max. stopband ripple magnitude [dB]	-70	-120
Optimization technique	Least-squares	Minimax

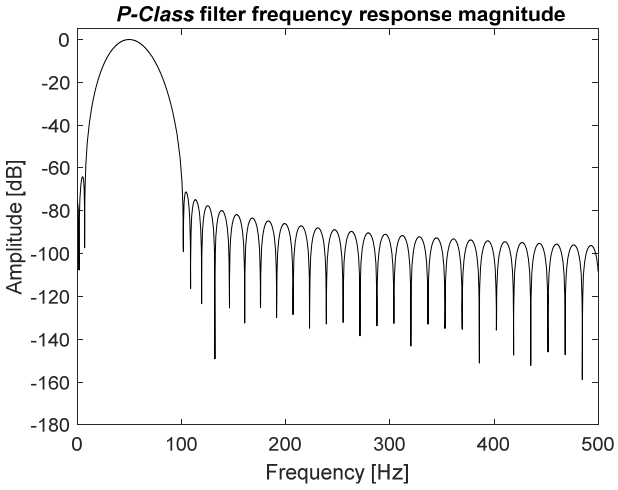

(a)

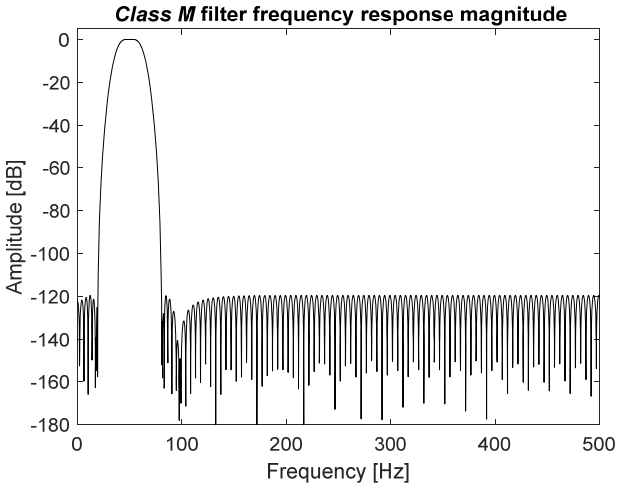

(b)

Fig. 2 – Magnitude of the frequency response of a *Class P* (a), and a *Class M* (b) FIR filter removing wideband and narrowband disturbances prior to applying the Teager's algorithm.

V. SIMULATION RESULTS IN THE TESTING CONDITIONS OF THE IEEE STANDARDS C37.118.1 AND C37.118.1A

The accuracy of the estimation algorithm based on Teager's operator after applying either filter described in Section IV was analyzed through Monte Carlo simulations in most of the *Class P* and *Class M* testing conditions reported in [23], [24], i.e. considering

a. signals with off-nominal static frequency deviations within ±2 Hz (*Class P*) or ±5 Hz (*Class M*) and voltage amplitudes between 80% and 120% or between 10% and 120% of the rated value, respectively;

b. signals affected by the same off-nominal frequency deviations as in case *a* and up to 50 harmonics (considered one at a time) of amplitude equal to 1% (*Class P*) or 10% (*Class M*) of the fundamental tone;

c. AM signals with a modulating tone frequency up to 2 Hz (*Class P*) or 5 Hz (*Class M*) and amplitude equal to 10% of the fundamental component;

TABLE II - MAXIMUM TVE, FE AND RFE VALUES IN *CLASS P* TESTING CONDITIONS OBTAINED I) FROM (7)-(10) AFTER BANDPASS FILTERING ONLY AND II) BY AVERAGING THE PREVIOUS SAMPLE-BY-SAMPLE DATA OVER 1-CYCLE-LONG INTERVALS. THE LIMITS REPORTED IN IEEE STANDARD C37.118.1-2011 OR IN THE AMENDMENT C37.118.1A-2014 FOR A REPORTING RATE OF 50 FPS ARE ALSO SHOWN FOR THE SAKE OF COMPARISON.

	Test type	TVE_{max} **[%]**			FE_{max} **[mHz]**			RFE_{max} **[Hz/s]**		
		Limit	**No avg.**	**With avg.**	**Limit**	**No avg.**	**With avg.**	**Limit**	**No avg.**	**With avg.**
a	Freq. dev. only (±2 Hz)	1	0.89	0.89	5	0.0	0.0	0.4	0.0	0.0
b	Freq. dev.+ 1% harmonics	1	0.98	0.98	5	24.	0.3	0.4	149.7	1.2
c	AM (f_a=2 Hz, k_a=10%)	3	0.15	0.14	60	7.3	4.8	2.3	1.6	0.1
d	PM (f_p=2 Hz, k_p=0.1 rad)	3	0.06	0.06	60	2.5	0.9	2.3	1.4	0.1
e	Frequency ramp[1] (±2 Hz @ ±1 Hz/s)	1	0.89	0.89	10	1.8	0.7	0.4	1.0	0.1
f	Wideband noise (*SNR* = 60 dB)	-	0.04	0.04	-	3.5	2.2	-	11.8	0.3

[1]Results obtained considering an exclusion interval of 40 ms (i.e., twice the maximum mandatory reporting period at 50 Hz) at the beginning and at the end of the ramp.

TABLE III - MAXIMUM TVE, FE AND RFE VALUES IN *CLASS M* TESTING CONDITIONS OBTAINED I) FROM (7)-(10) AFTER BANDPASS FILTERING ONLY AND II) BY AVERAGING THE PREVIOUS SAMPLE-BY-SAMPLE DATA OVER 1-CYCLE-LONG INTERVALS. THE LIMITS REPORTED IN IEEE STANDARD C37.118.1-2011 OR IN THE AMENDMENT C37.118.1A-2014 FOR A REPORTING RATE OF 50 FPS ARE ALSO SHOWN FOR THE SAKE OF COMPARISON.

	Test type	TVE_{max} **[%]**			FE_{max} **[mHz]**			RFE_{max} **[Hz/s]**		
		Limit	**No avg.**	**With avg.**	**Limit**	**No avg.**	**With avg.**	**Limit**	**No avg.**	**With avg.**
a	Freq. dev. only (±5 Hz)	1	0.59	0.59	5	0.0	0.0	0.1	0.0	0.0
b	Freq. dev.+ 10% harmonics	1	1.00	0.98	25	71.1	0.6	-	414	3.8
c	AM (f_a=5 Hz, k_a=10%)	3	0.57	0.55	300	68.0	44.3	14	14	1.8
d	PM (f_p=5 Hz, k_p=0.1 rad)	3	0.12	0.12	300	22.8	6.0	14	13	0.6
e	Frequency ramp[2] (±5 Hz @ ±1 Hz/s)	1	0.65	0.62	10	2.0	0.2	0.2	1.0	0.1
f	Wideband noise (*SNR* = 60 dB)	-	0.02	0.02	-	1.4	1.2	-	2.7	0.1
g	10% Out-of-band inter-harmonics	1.3	0.04	0.04	10	18.1	9.9	-	4.8	1.8

[2]Results obtained considering an exclusion interval of 140 ms (i.e., 7 times the maximum mandatory reporting period at 50 Hz) at the beginning and at the end of the ramp.

d. PM signals with a modulating tone frequency up to 2 Hz (*Class P*) or 5 Hz (*Class M*) and amplitude equal to 0.1 rad;

e. chirp signals with frequency changing linearly between 48 Hz and 52 Hz (*Class P*) or between 45 Hz and 55 Hz (*Class M*) at a rate of ±1 Hz/s;

f. a pure sinewave affected by wideband noise, so that *SNR* = 60 dB (this testing condition is not considered in the IEEE Standards, but it is interesting due to the high sensitivity of the estimation algorithm to noise, as explained in Section IV);

g. signals affected by out-of-band inter-harmonic tones of amplitude equal to 10% of the fundamental and frequency within [10 Hz, 25 Hz] or [75 Hz, 100 Hz], assuming a reporting rate of 50 fps (*Class M* only).

The Monte Carlo simulations were performed following the same approach described in Section III, i.e. by generating 50 signals of 5 s each (except in the *Class M* chirp case, which requires at least 10-second signals) with initial phases chosen at random in [0, 2π] and for different waveform parameters depending on the specific testing conditions considered. Again, $f_s = 6.4$ kHz, $X = \sqrt{2}$ p.u., $f_0 = 50$ Hz. The maximum TVE, FE and RFE values resulting from simulations are reported in Tab. II and III, for *Class P* and *Class M* conditions, respectively, along with the limits specified in [23] or [24] for a reporting rate of 50 fps. Besides the results related to sample-by-sample estimates, the values of TVE, FE and RFE obtained by averaging synchrophasor magnitude, frequency and ROCOF data over one-cycle intervals are shown.

Observe that, in general, the output average does not have a significant impact on TVE, since the average operator tends to smooth the tracking ability of the dynamic estimator. This is not a problem, since the TVE limits reported in the IEEE Standards are met in both *Class P* and *Class M* conditions, although the maximum TVE values in the presence of harmonics are borderline. On the contrary, the values of FE and RFE obtained by averaging the sample-by-sample estimates over one-cycle intervals are smaller (and sometimes much smaller) than those obtained when no average is applied. This behavior is particularly evident in the presence of large steady-state disturbances, such as harmonics or inter-harmonics. Therefore, the band-pass filters alone, although effective in making the effect of wideband noise negligible on

estimated results, are not sufficient to meet the FE and RFE limits of the IEEE Standards when heavily distorted waveforms are considered. The output one-cycle average addresses this problem easily in almost all conditions. In fact, only the *Class P* RFE limit in the presence of harmonics is occasionally exceeded.

A further analysis that, due to space constraints, will be expanded in a future work, concerns with the ability of the proposed *Class P* and *Class M* FIR filters to extract the In-phase and Quadrature (I/Q) components of the input digitized waveform, in order to estimate synchrophasor magnitude and phase directly from such components. Some preliminary results show that the TVE values obtained with this alternative approach are generally comparable with those reported in Tabs. II and III. However, using the filter-based approach both frequency and ROCOF (namely the first- and second-order derivatives of the instantaneous phase) should be estimated by applying Euler differences once and twice, respectively. On the contrary, the Teager's operator returns the waveform frequency directly from (7). Therefore, in this case the Euler difference derivative estimator (which is notoriously quite sensitive to noise) can be applied just to estimate the ROCOF.

VI. Conclusion

The time-domain estimation algorithm based on the Teager's energy operator (originally conceived to track the energy of time-varying audio signals) can be successfully used to measure amplitude, phase, frequency and ROCOF of voltage or current waveforms under dynamic conditions. The main benefits of the Teager-based approach area low computational burden and the ability to return estimates with a sample-by-sample time resolution. Its main drawback instead is the high sensitivity to noise and disturbances. This problem can be addressed (at the expense of an increment of computational burden) in two complementary ways, i.e. i) by using ad-hoc bandpass filters to attenuate both narrowband and wideband disturbances before waveform parameters estimation and ii) by averaging the sample-by-sample frequency and ROCOF estimates over at least one power line cycle.

References

[1] A. G. Phadke, J. S. Thorp, and M. G. Adamiak, "A new measurement technique for tracking voltage phasors, local system frequency, and rate of change of frequency," *IEEE Trans, on Power Apparatus and Systems*, vol. PAS-102, no. 5, pp. 1025–1038, May 1983.

[2] D. M. Laverty, R. J. Best and D. J. Morrow, "Loss-of-mains protection system by application of phasor measurement unit technology with experimentally assessed threshold settings," in *IET Generation, Transmission & Distribution*, vol. 9, no. 2, pp. 146-153, 29 1 2015.

[3] M. Pignati, L. Zanni, P. Romano, R. Cherkaoui, and M. Paolone, "Fault detection and faulted line identification in active distribution networks using synchrophasors-based real-time state estimation," *IEEE Trans. on Power Delivery*, vol. 32, no. 1, pp. 381–392, Feb. 2017.

[4] A. Shahsavari *et al.*, "Distribution Grid Reliability Versus Regulation Market Efficiency: An Analysis Based on Micro-PMU Data," in *IEEE Trans. on Smart Grid*, vol. 8, no. 6, pp. 2916-2925, Nov. 2017.

[5] D. Macii, G. Barchi and D. Moser, "Impact of PMUs on state estimation accuracy in active distribution grids with large PV penetration," Proc. *2015 IEEE Workshop on Environmental, Energy, and Structural Monitoring Systems* (EESMS), Trento, Italy, Ju. 2015, pp. 72-77.

[6] P. Castello, P. Ferrari, A. Flammini, C. Muscas and S. Rinaldi, "A New IED With PMU Functionalities for Electrical Substations," in *IEEE Trans. on Instr. and Meas.*, vol. 62, no. 12, pp. 3209-3217, Dec. 2013.

[7] G. Barchi, D. Fontanelli, D. Macii and D. Petri, "On the Accuracy of Phasor Angle Measurements in Power Networks," *IEEE Trans. on Instr. and Meas.*, vol. 64, no. 5, pp. 1129-1139, May 2015.

[8] J. A. de la O Serna, "Dynamic Phasor Estimates for Power System Oscillations," in *IEEE Trans. on Instr. and Meas.*, vol. 56, no. 5, pp. 1648-1657, Oct. 2007.

[9] M. Platas-Garza and J. de la O Serna, "Dynamic phasor and frequency estimates through maximally flat differentiators," *IEEE Trans. on Instr. and Meas.*, vol. 59, no. 7, pp. 1803–1811, Jul. 2010.

[10] D. Belega, D. Fontanelli, D. Petri, "Dynamic phasor and frequency measurements by an improved taylor weighted least squares algorithm," in *IEEE Trans. on Instr. and Meas.*, vol. 64, no. 8, pp. 2165-2178, Aug. 2015.

[11] D. Petri, D. Fontanelli, and D. Macii, "A frequency-domain algorithm for dynamic synchrophasor and frequency estimation," *IEEE Trans. on Instr. and Meas.*, vol. 63, no. 10, pp. 2330–2340, Oct. 2014.

[12] M. A. Platas-Garza and J. A. de la O Serna, "Dynamic harmonic analysis through Taylor-Fourier transform," *IEEE Trans. on Instr. and Meas.*, vol. 60, no. 3, pp. 804–813, Mar. 2011.

[13] M. D. Kušljević and J. J. Tomić, "Multiple-resonator-based power system Taylor-Fourier harmonic analysis," *IEEE Trans. on Instr. and Meas.*, vol. 64, no. 2, pp. 554–563, Feb. 2015.

[14] D. Macii and D. Petri, "Harmonics Estimation in Transient Conditions using Static and Dynamic Frequency-domain Techniques," Proc. *IEEE 9th International Workshop on Applied Measurements for Power Systems* (AMPS), Bologna, Italy, Sep. 2018.

[15] J. Liu, F. Ni, J. Tang, F. Ponci, and A. Monti, "A Modified Taylor-Kalman Filter for Instantaneous Dynamic Phasor Estimation," in Proc. *IEEE PES Innovative Smart Grid Technologies Europe* (ISGT Europe), Berlin, Germany, Oct. 2012, pp. 1–7.

[16] D. Fontanelli, D. Macii and D. Petri, "Dynamic synchrophasor estimation using Smoothed Kalman filtering," Proc. *IEEE Int. Instr. and Meas. Tech. Conf.* (I2MTC), Taipei, Taiwan, May 2016, pp. 1-6.

[17] R. Ferrero, P. A. Pegoraro, and S. Toscani, "Dynamic Fundamental and Harmonic Synchrophasor Estimation by Extended Kalman Filter," Proc. *IEEE Int. Workshop on Applied Measurements for Power Systems* (AMPS), Aachen, Germany, Sep. 2016, pp. 1–6.

[18] M. Bertocco, G. Frigo, C. Narduzzi, C. Muscas and P. A. Pegoraro, "Compressive Sensing of a Taylor-Fourier Multifrequency Model for Synchrophasor Estimation," in *IEEE Trans. on Instr. and Meas.*, vol. 64, no. 12, pp. 3274-3283, Dec. 2015.

[19] P. Tosato, D. Macii, M. Luiso, D. Brunelli, D. Gallo and C. Landi, "A Tuned Lightweight Estimation Algorithm for Low-Cost Phasor Measurement Units," in *IEEE Trans. on Instr. and Meas.*, vol. 67, no. 5, pp. 1047-1057, May 2018.

[20] D. M. Laverty, J. Hastings, D. J. Morrow, R. Khan, K. Mclaughlin and S. Sezer, "A modular phasor measurement unit design featuring open data exchange methods," Proc. *IEEE Power & Energy Society General Meeting*, Chicago, IL, Jul. 2017, pp. 1-5.

[21] J. F. Kaiser, "On a simple algorithm to calculate the 'energy' of a signal," Proc. *IEEE International Conference on Acoustics, Speech, and Signal Processing*, Albuquerque, NM, USA, Aug. 1990, pp. 381-384.

[22] P. Maragos, J. F. Kaiser and T. F. Quatieri, "Energy separation in signal modulations with application to speech analysis," in *IEEE Trans. on Sig, Proc.*, vol. 41, no. 10, pp. 3024-3051, Oct. 1993.

[23] IEEE Std. C37.118.1-2011, *IEEE standard for synchrophasor measurements for power systems*, pp. 1–61, Dec. 2011.

[24] IEEE Std C37.118.1a-2014 (Amendment to IEEE Std C37.118.1-2011), *IEEE standard for synchrophasor measurements for power systems – amendment 1: Modification of selected performance requirements*, pp. 1–25, Apr. 2014.

[25] M. Luiso, D. Macii, P. Tosato, D. Brunelli, D. Gallo and C. Landi, "A Low-Voltage Measurement Testbed for Metrological Characterization of Algorithms for Phasor Measurement Units," in *IEEE Trans. on Instr. and Meas.*, vol. 67, no. 10, pp. 2420-2433, Oct. 2018.

[26] D. Macii, G. Barchi and D. Petri, "Design criteria of digital filters for synchrophasor estimation," Proc. *IEEE Int. Instr. and Meas. Tech. Conf.* (I2MTC), Minneapolis, MN, May 2013, pp. 1579-1584.